Aeroheating Analysis for the Mars Reconnaissance Orbiter with Comparison to Flight Data

Derek S. Liechty[1]
NASA Langley Research Center, Hampton, VA 23681

The aeroheating environment of the Mars Reconnaissance Orbiter (MRO) has been analyzed using the direct simulation Monte Carlo and free-molecular techniques. The results of these analyses were used to develop an aeroheating database to be used for the pre-flight planning and the in-flight operations support for the aerobraking phase of the MRO mission. The aeroheating predictions calculated for the MRO include the heat transfer coefficient (C_H) over a range of angles-of-attack, sideslip angles, and number densities. The effects of flow chemistry, surface temperature, and surface grid resolution were also investigated to determine the aeroheating database uncertainties. Flight heat flux data has been calculated from surface temperature sensor data returned to Earth from the MRO in orbit around Mars during the aerobraking phase of its mission. The heat flux data have been compared to the aeroheating database and agree favorably.

Nomenclature

C_H	=	heat transfer coefficient, $C_H = q/(0.5\rho_\infty V_\infty^3)$
c_p	=	specific heat
k	=	thermal conductivity
n_∞	=	free stream number density
q	=	surface heat transfer rate
T_∞	=	free stream temperature
V_∞	=	free stream velocity magnitude
α	=	angle-of-attack
β	=	side-slip angle
ε	=	emissivity
λ_∞	=	free stream mean free path
ρ_∞	=	free stream density
ρ_s	=	solar cell substrate density

I.   Introduction

The Mars Reconnaissance Orbiter (MRO) was launched on August 12, 2005. It has delivered to Mars orbit a payload to conduct remote sensing science observations, identify and characterize sites for future landers, and provide critical telecom/navigation relay capability for follow-on missions. During the one Martian year (687 Earth days) primary science phase, the orbiter will acquire visual and near-infrared high-resolution images of the planet's surface, monitor atmospheric weather and climate, and search the upper crust for evidence of water. After the science phase is completed, the orbiter will provide telecommunications support for spacecraft launched to Mars in

---

[1] Aerospace Engineer, Aerothermodynamics Branch, m/s 408A, AIAA Member.

the 2007 and 2009 opportunities. The primary mission ends on December 31, 2010, approximately 5.5 years after launch.

After Mars insertion, the aerobraking phase started with a series of "walk-in" maneuvers. The strategy was to gradually bring the periapsis altitude to a level such that the dynamic pressure and heating rate satisfy pre-set corridor conditions for the main aerobraking phase. While the periapsis altitude was within the upper bound of the Martian atmosphere, the spacecraft experienced deceleration induced by atmospheric drag. In about six months, the orbit period was reduced to about 2 hours from a 35-hour initial orbit period. The total energy savings was equivalent to about 1200 m/s in ΔV_∞.

All of the aerobraking took place at altitudes where the densities were sufficiently low that the flow was in the rarefied transitional regime. To accurately predict the aeroheating characteristics of the spacecraft in the rarefied transitional regime, the direct simulation Monte Carlo (DSMC) and free molecular techniques were used. The results from the calculations were used to create the aeroheating database of the spacecraft.

Flight operations support was also provided throughout the aerobraking maneuver. Temperature sensor data, along with atmospheric data, was transmitted to Earth from the MRO and heating rates at specific temperature sensor locations were calculated. The procedures used to calculate the in-flight heat flux and sample flight data are presented herein. Comparisons between the aeroheating database and the calculated, in-flight values are favorable.

II.   Computational Methods

The DSMC calculations were performed using DDAC, the parallel implementation of the program DAC (DSMC Analysis Code).[1,2] In DAC, the gas molecular collisions are modeled using the variable-hard-sphere (VHS) model developed by Bird[3], and the Larsen-Borgnakke model is used for internal energy exchanges[4]. The surface geometry is represented by unstructured triangular elements that are embedded in a two-level Cartesian grid for the flow field calculation. The solution from the first level of grid cells, which are uniform in size, is used for grid refinement to create the second-level cells. The grid is refined based on local conditions, thus allowing the program to meet the spatial resolution requirements without excessive global refinement. The grid cells are typically refined such that on average the second-level cells have dimensions less than the local mean free path. This restriction was obtained for the densities expected in flight (four additional, higher densities were simulated for thermal limit lines). The local simulation parameters are set such that there are nominally 10 simulated molecules in each cell, and the local time

step is typically dictated by the local flow time for the problems considered. The number of time steps until steady state was set to 5000, followed by enough sampling time steps to allow most of the surface triangular elements to accumulate at least 1000 molecular collisions (this was the lower limit for small surface elements; most surface elements had on the order of a few million molecular impacts), resulting in a total of somewhere on the order of 30,000 steady state time steps.

For all calculations, the wall collisions were assumed to be fully diffusive, i.e., an accommodation coefficient of one was specified, with the spacecraft wall temperature at a constant 300 K. The composition of Mars atmosphere was assumed to be 95.37% CO_2 and 4.63% N_2 by mole with a free stream temperature of 144.7 K and velocity of 4811.0 m/s for densities below 100 kg/km^3, decreasing to 3611 m/s at a density of approximately 350 kg/km^3. The decreases in velocity at the higher number densities represent the larger ΔV_∞ that would be experienced at these conditions. However, these number densities are not expected and were included in the database to assist the Langley MRO Thermal Team to develop the spacecraft thermal limit lines.

The computational geometry shown in Fig. 1 was derived from a CAD file provided by Lockheed Martin Astronautics (LMA) and represents the best pre-flight estimate of the nominal aerobraking configuration. The spacecraft itself is about 12 meters wide from the outside tip of one solar panel to the other. Special care was taken to accurately represent the science modules for aerobraking analysis, as shown in Fig. 1.b. Free stream conditions for all number densities simulated can be viewed in Table 1. The shaded rows indicate free stream conditions that are not expected in flight, but were included in the database to help the LaRC Thermal Team define thermal limit lines. At each density, angles-of-attack and sideslip angles of -10, 0, and +10-degrees were also simulated.

Free molecular results were obtained using DACFREE[5]. DACFREE is a companion code to DAC, which utilized the same unstructured triangular surface mesh. The free molecular forces, moments, and heat transfer rates were calculated at each surface triangular element with analytical free-molecular analysis[3] and line-of-sight shadowing was enforced to ensure that only those surface elements exposed to the free stream flow contribute to the total values of force, moment, and heat transfer for the entire vehicle. These individual contributions from the surface elements were then summed, resulting in the values for the spacecraft as a whole.
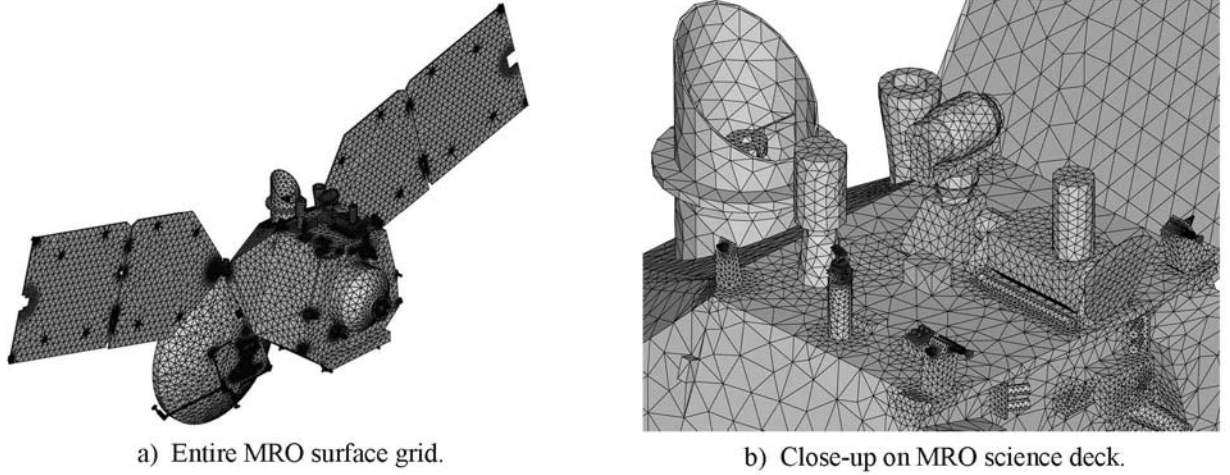
a) Entire MRO surface grid.

b) Close-up on MRO science deck.

Fig. 1 MRO computational surface geometry.

Table 1. Free stream conditions

n_∞	ρ_∞ (kg/m^3)	V_∞ (m/s)	T_∞ (K)	λ_∞ (m)
7.795e16	5.6007e-9	4811	144.77	7.63
1.392e17	1.0001e-8	4811	144.77	4.27
2.475e17	1.7783e-8	4811	144.77	2.40
4.402e17	3.1628e-8	4811	144.77	1.35
1.392e18	1.0001e-7	4811	144.77	0.42
2.088e18	1.5002e-7	4211	144.77	0.28
3.480e18	2.5004e-7	3911	144.77	0.17
4.872e18	3.5005e-7	3611	144.77	0.12

III.   Database Uncertainty Analysis

As with any database, some uncertainty must be assigned to the heating levels presented herein. While some uncertainties are generalized and apply to any data set, there were several that needed to be quantified for the present database. These are analyzed and discussed below.

A. Effect of Chemical Reactions

The importance of including chemical reactions must be analyzed. A 2-species, non-reacting chemistry model was compared to a 9-species, reacting chemistry model at the highest expected density to be experienced in flight (32 kg/km^3). The variation of the non-dimensional incident heating coefficient, C_H, is compared along the centerline of one of the solar panels of the MRO for the reacting and non-reacting cases in Fig. 2 vs. distance from the root of the panel. The incident heating rates between the reacting and non-reacting flow cases differed by only a couple of percentage points. Therefore, it was determined that the addition of chemical reactions does not significantly effect

the heating rate and was not included in the database. The maximum difference was estimated to be less than 5% at the edges of the solar panels.
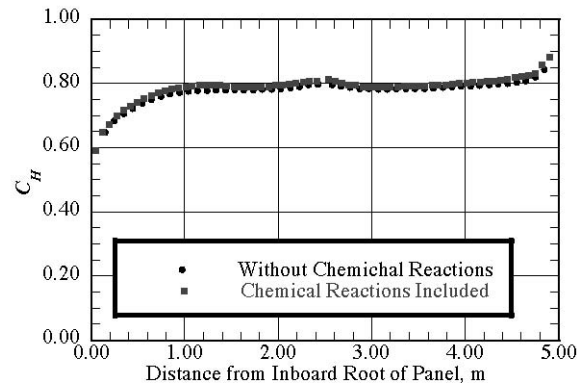

Fig. 2 Comparison of incident heating along the solar panel centerline with and without chemistry effects.

B. Effect of Surface Grid Resolution

The next uncertainty examined was the effect of changing the surface grid resolution at the highest expected density to be experienced in flight ($32 \ kg/km^3$). The nominal surface grid was compared to a surface grid for which the size of the surface elements was decreased by approximately one half once again at the maximum expected density at zero-degrees angle-of attack and side-slip. The corresponding centerline cuts through one of the solar panels can be viewed in Fig. 3. The greatest differences observed were near the corners of the solar panels and was estimated to be less than 1%.
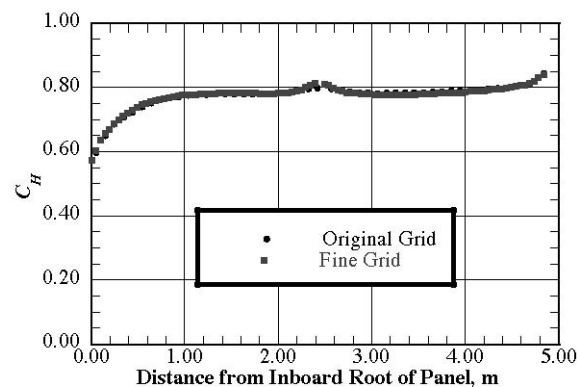

Fig. 3 Comparison of incident heating along the solar panel centerline for original grid and fine grid.

C. Effect of Surface Temperature

The final simulation parameter to be examined for uncertainty is the variation of the incident heating rate with the wall temperature specified for the spacecraft at the highest expected density to be experienced in flight (32 kg/km^3). The nominal wall temperature was chosen to be 300 K. Off-nominal surface temperatures of 150 K and 600 K were chosen for comparison along the solar panel centerline. The value of 600 K was obviously higher than any expected in-flight temperature, but is included to get the maximum uncertainty level. As it turns out, the 150 K off-nominal temperature was lower than any of the temperatures observed near the atmospheric entry portion of the aerobraking maneuver, but provided a reasonable lower bound. The corresponding centerline cuts through one of the solar panels can be viewed in Fig. 4. The greatest difference was approximately 5%.
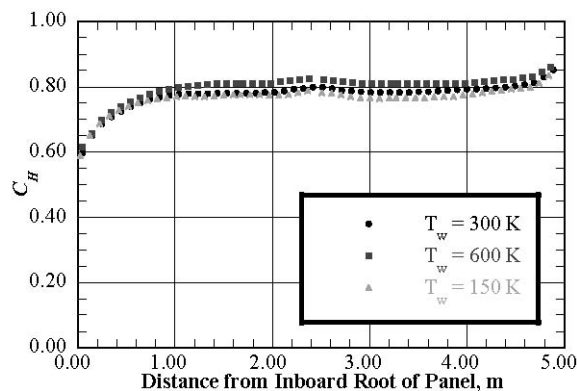

Fig. 4   Comparison of incident heating along the solar panel centerline for varying spacecraft surface temperature.

D. Summary of Database Uncertainty

A summary of the uncertainties included in the overall estimate of database uncertainty is shown in Table 2. The main sources of uncertainty are computational errors (statistical sampling, gridding errors), physical model errors (gas collision model used, accommodation coefficient used, chemical reactions), boundary conditions (atmospheric temperature, surface temperature), and any errors in the computational geometry model used (whether or not the multi-layer insulation was applied correctly, simplifications to some parts, etc.). While this may not be an all-inclusive list of possible sources of error, the major contributors have been included and examined.

The database uncertainty was reported with and without the inclusion of the accommodation coefficient uncertainty. The thermal analysis team at the NASA Langley Research Center used the uncertainty without this value because their analysis did not include the reflected heating rate, only the incident heating rate. The accommodation coefficient affects the incident heating only slightly (by varying the number density near the

surface). The other uncertainty reported including the uncertainty due to the accommodation coefficient will be used in the remainder of this report to compare the database to flight data. Both uncertainties were calculated by taking the square root of the sum of the squares of the contributing uncertainties.

The grid, chemical reaction, and surface temperature have already been addressed above. The statistical sampling error was estimated by approximating the uncertainty as $1/\sqrt{N}$, where N is the number of surface collisions. Since most of the surface elements accumulated on the order of one million surface collisions, this uncertainty was estimated to be ±0.1%. The gas collision model, accommodation coefficient, and atmospheric temperature uncertainties are historical values that have been used with confidence in previous planetary missions. The geometry error was an uncertainty that was difficult to assign a value to. This uncertainty is only mentioned and was not assigned a value since a direct comparison between the computational model and the spacecraft in flight cannot be made. The final database uncertainties are therefore assigned values of ±7.9% and ±9.4% with and without the inclusion of the accommodation coefficient uncertainty, respectively.

Table 2. Influences on aeroheating database uncertainties.

Source of Uncertainty	Relative Effect on C_H
Computational Errors	
Statistical Sampling	±0.1%
Grid	±3%
Physical Model Errors	
Gas Collision Models	±2%
Accommodation Coefficient	±5%
Chemical Reactions	±5%
Boundary Conditions	
Atmospheric Temperature	±0.2%
Surface Temperature	±5%
Geometry	Small
RMS Uncertainty (Excl. Acc. Coef.)	±7.9%
RMS Uncertainty (Incl. Acc. Coef.)	±9.4%

IV.   Review of the Aeroheating Database

A. Effect of Varying Density

Due to the elliptical orbit of the MRO during the aerobraking phase of the mission, wide ranges of densities were encountered. As a lower limit, free molecular simulations were examined. The nominal maximum density that the MRO was to encounter was estimated to be 32 kg/km^3. Simulations of approximately 6, 10, 18, 32, 100, 150, 250, and 350 kg/km^3, as well as free molecular, were carried out in order to quantify the effect of the varying density

along the trajectory. Heating results for these densities at the nominal angle-of-attack and sideslip angle of 0-deg.
are presented in Fig. 5. Although the non-dimensionalized heating may be decreasing as density increases, it should
be noted that the actual heating rates are increasing since the density is also increasing. The value of C_H decreases
with density because the kinetic energy of the incident molecules is decreasing due to the increasing number of
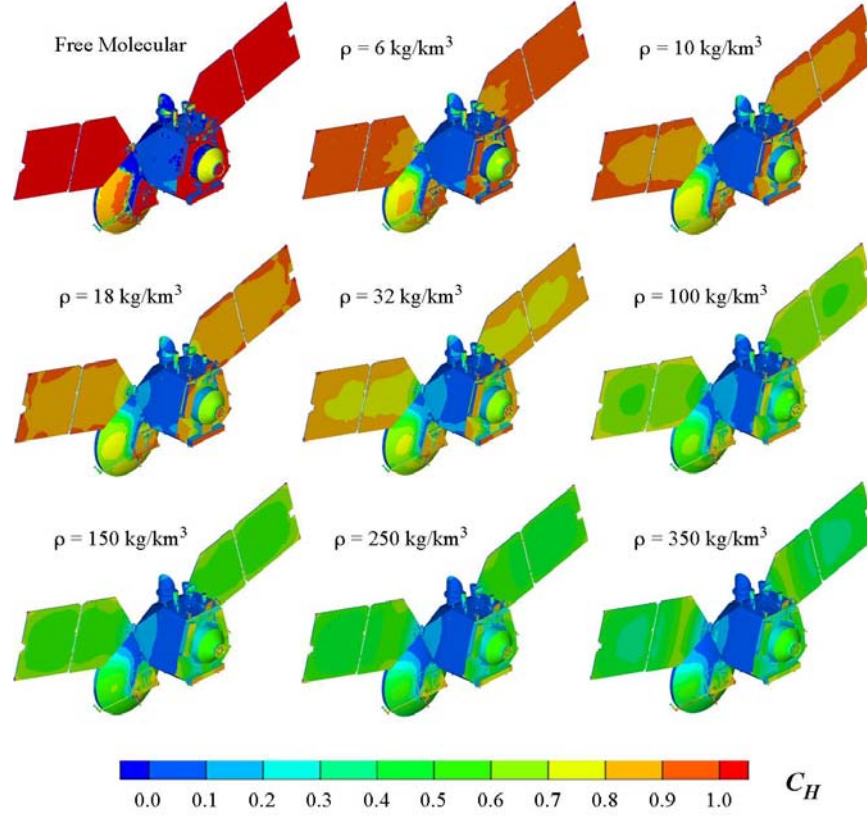collisions within the shock layer upstream of the spacecraft.

Fig. 5 Effect of density at $\alpha = 0$ deg, $\beta = 0$ deg.

B. Effect of Angle-of-Attack and Side-Slip

A variety of angles-of-attack and sideslip angles were examined in this study. Values of -10, 0, and +10-deg
were simulated for both of these parameters. A sample of these conditions is presented in Fig. 6 at the maximum
nominal density of 32 kg/km^3. The MRO passes through the atmosphere with the science instruments pointed
downward towards the surface of Mars, so in Fig. 6, Mars is "up." A positive angle-of-attack has therefore been
defined as having the MRO as seen in Fig. 6 rotate clockwise so that the science instruments are more directly into
the flow (the edge of the solar panels that experiences higher heating is pointed more directly into the flow).
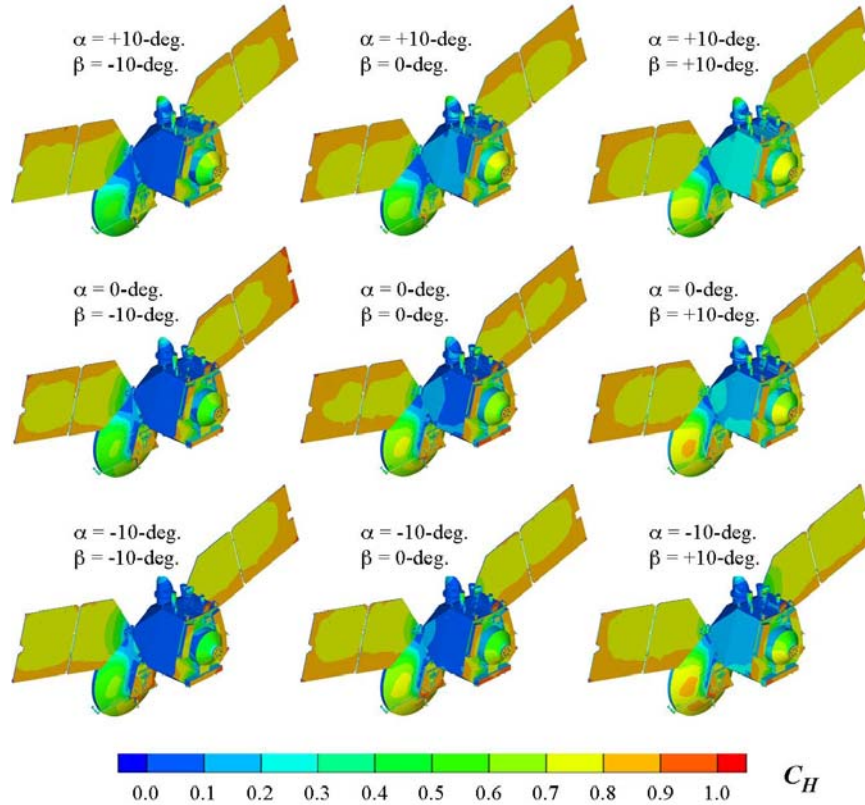
Fig. 6 Effect of angle-of-attack and sideslip at $\rho = 32$ kg/km^3.

V.   Comparison to Flight Data

As the MRO performed the aerobraking maneuver, engineers continually monitored flight data sent back to Earth to make sure that the MRO was going to complete aerobraking on time in the safest possible manner. One aspect of this monitoring process was the calculation of surface heat flux from surface temperature sensor data and the comparison of this in-flight heating rate with the aeroheating database. This was performed to provide updates to the aeroheating database when and if necessary. Three sensor locations on one of the solar panels were monitored. The sensor locations can be seen in Fig. 7. Sensors T-0109, T-0110, and T-0309 (outlined in grey) were the forward-facing temperature sensors. Sensor T-0310 (outlined in black) was the only temperature sensor on the back face of the solar array being monitored.
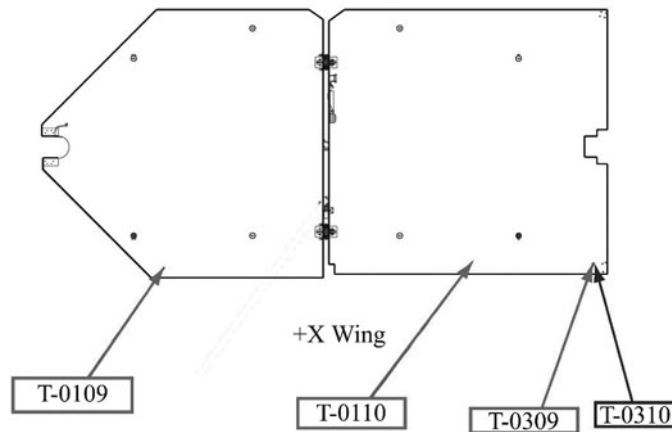
Fig. 7 Temperature sensor locations.

A. Method of Calculation of In-Flight Heat Transfer Rate

The heat flux due to atmospheric heating to the solar arrays at the three forward facing temperature sensor locations was calculated by modifying the code 1DHEAT[6], which is a one-dimensional heat transfer analysis tool. The finite-volume implementation of 1DHEAT takes direct account of the variable substrate thermal properties and removes the restriction of a semi-infinite substrate (thus allowing for a multiple layer analysis), which is important due to the structure of the solar panels. The code was modified to allow for prescribing the temperature on the back surface of the solar panels as a function of time and to allow for radiative boundary conditions on the front and back surfaces of the solar panels, including the orbital flux (solar, albedo, and Mars IR) input and radiative emission of energy for given absorptivity and emissivity, respectively. The values for orbital flux were obtained from the Thermal Team and accounted for spacecraft attitude, incidence angle, shading from the spacecraft main bus, and reflection from the rest of the vehicle.

The material and the corresponding thickness for each layer of the solar panels can be seen in Table 3. A representation of the problem of interest can also be viewed in Fig. 8. There are a total of five layers to be accounted for (adhesives are neglected in this analysis). It should be noted that the total thickness of the inboard panel is greater than that of the outboard panel. The solar cell material thermal properties are presented in Table 4. Although the Al HC is a honeycomb material, it was treated as a solid layer with properties equivalent to the honeycomb structure (similar to the methods followed by the Thermal Team).

Table 3. Material and thickness of solar panel layers.

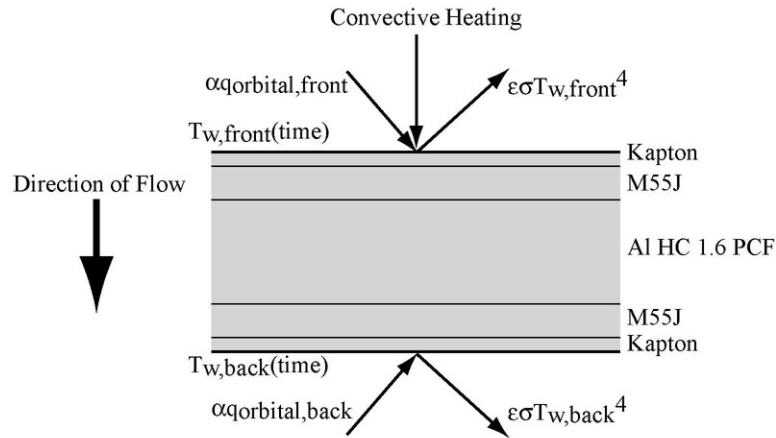| Layer	Material	Thickness (m) (T-0109)	Thickness (m) (T-0110, T-0309)
1	Kapton	7.6e-5	7.6e-5
2	M55 J/RS-3	5.0e-4	2.5e-4
3	Al HC 1.6 PCF	2.9e-2	2.26e-2
4	M55 J/RS-3	5.0e-4	2.5e-4
5	Kapton	5.0e-5	5.0e-5

Fig. 8 Depiction of in-flight aeroheating problem with all inputs/outputs considered.

Table 4. Solar panel material properties.

Material	ρ_s (kg/m^3)	c_p (J/ kg K)	k (W/ m K)	ε
Kapton	1450	1000	0.1557	0.75
M55 J/RS-3	1700	795	1.0	---
Al HC 1.6 PCF	28	830	0.9	---

B. In-Flight Uncertainties

The uncertainties in the calculation of the in-flight convective heating must now be quantified. There are several potential sources of uncertainty that were examined: orbital radiative heat flux, solar panel substrate thermal properties, and the temperature to which the solar panel was radiating. The quoted uncertainty (3-σ) or range of values tested (where a quoted uncertainty was not available) and the impact on surface convective heating for these variables are listed in Table 5. These uncertainties result in a square root of the sum-of-the-squares flight uncertainty of about ±30%. There are, of course, other sources of uncertainty that are not listed in Table 5 such as

the uncertainty in kapton thermal properties, material density, etc. The values of uncertainty on these properties were not quoted and are therefore not included.

Table 5. Sources of uncertainty and their effect on in-flight convective heating rate.

Uncertainty Source	3-σ Uncertainty / Range Tested	Effect on C_H
Solar Heat Flux	±30%	±10%
Kapton Emmisivity	±10%	±10%
M55 J Thermal Conductivity	±25%	±5%
M55 J Specific Heat	±15%	±5%
Al HC Thermal Conductivity	±30%	±25%
Al HC Specific Heat	±5%	±1%
Ambient Temperature (Radiated To)	0 K – 100 K	±5%

C. In-Flight Raw Data

The measured surface temperatures of the three forward-facing temperature sensors as well as the estimated radiative heat flux to each sensor are presented in Fig. 9.a. The Langley MRO Thermal Team estimated the radiative heat flux by taking into account inputs from the Sun, Mars, and solar albedo as the spacecraft orbits Mars. There was only one temperature sensor available for the rear-facing boundary conditions, T-0310, which is located almost directly on the other side of the solar panel from T-0309. In order to obtain reasonable back-face temperatures for T-0109 and T-0110, it was assumed that the back surface temperature distributions roughly resembled the forward surface temperature distributions, anchored to T-0310. Therefore, for example, to calculate the back face temperature for T-0109, the temperature at T-0310 was multiplied by the ratio of the temperatures at T-0109 and T-0309. The author acknowledges that this assumption was not based on the physics of the problem, but was only intended as an engineering estimate since flight data was not available for the other two sensors. The radiative heat flux at T-0310 was used for the back face radiative inputs for T-0109 and T-0110, as well. The back face temperatures and heat flux used are presented in Fig. 9.b.
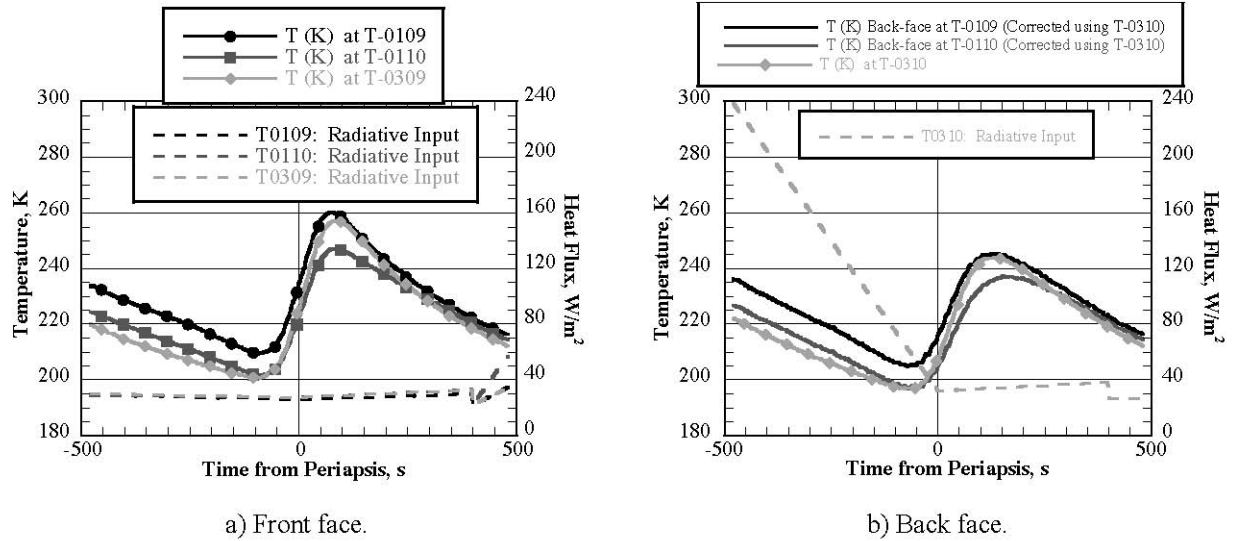
a) Front face.

b) Back face.

Fig. 9 Surface temperature and radiative heat flux inputs for orbit 27.

D. In-Flight Heat Transfer Rate and Comparison to Aeroheating Database

The calculated in-flight heat flux from temperature sensor T-0309, along with the predicted pre-flight values from the database, is presented in Fig. 10. Although in-flight calculations for the other two forward facing temperature sensors were performed, they are omitted from the figure for clarity since the results are similar to the temperature sensor shown. The heat flux is shown in units of W/cm^2 because these are generally the units used when presenting heating data on planetary entry systems. The predicted heat flux was interpolated from the database as a function of spacecraft orientation and density by way of a second order Lagrangian interpolation subroutine. The ±10% uncertainty is shown as two thin black lines on either side of the database values. Outside of the atmosphere (for this orbit, the spacecraft is within the sensible atmosphere between approximately 150 seconds before and after periapsis), the convective heating should be equal to zero. The values that were calculated for orbit 27 are within ±0.01 W/cm^2 of the expected value of zero with a positive slope to the heat flux as the MRO approached the atmosphere. This may be due to slightly incorrect values of orbital heat flux or some variability in material thermal properties (incorrect values or values that change with temperature). Part of this discrepancy could also be due to the change in temperature that the solar panels are radiating to. The value pre-set in this study was 10 K, but if this value were increasing with time, the heating rate would decrease along the trajectory. Another consideration is that the code used in this analysis uses the assumption of one-dimensional conduction. If there were any temperature gradients span-wise across the solar panels, the accuracy of the computed heat flux would decrease.
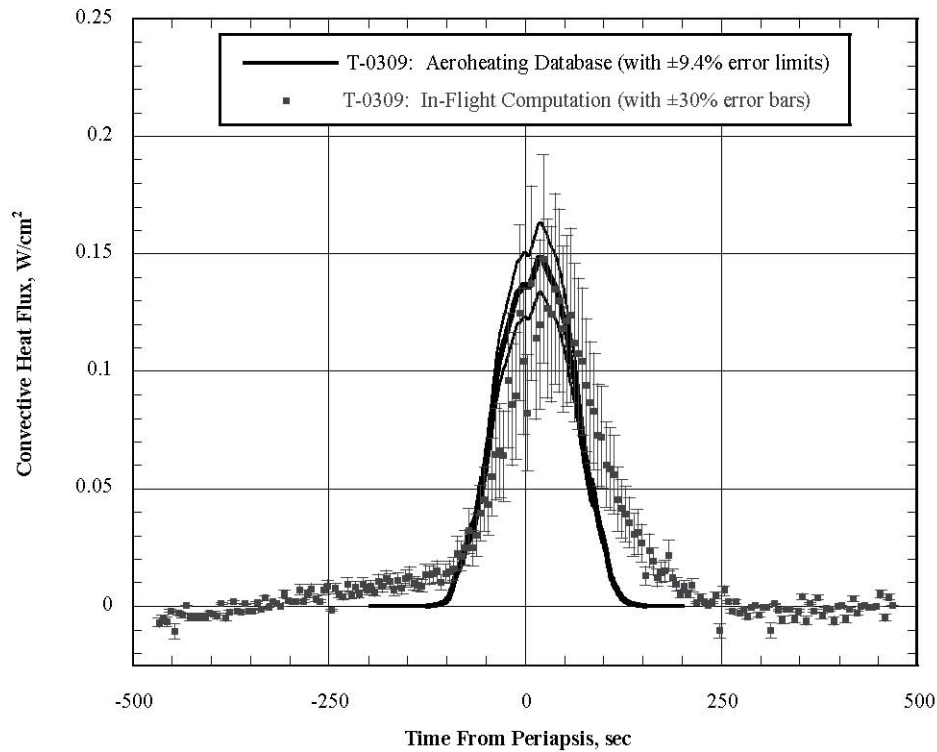
Fig. 10   Comparison of aeroheating database with computed in-flight heat flux (T-0309; orbit 27).

The computed heat flux also appears to lag behind the predicted values of heat flux as the spacecraft passes through the atmosphere, which may also be attributable to slightly incorrect thermal properties or thermal gradients. The calculated peak heating rate was about 15-20% lower than the predicted value. This could either once again be due to thermal properties, thermal gradients, or due to the fact that the accommodation coefficient for a spacecraft is almost always less than one[7], which was used in the development of the database. The lower the accommodation coefficient, the lower the convective heating rate would be. However, due to the uncertainties in the boundary conditions and structural thermal properties, one must be careful in drawing conclusions such as these based on such a small difference in heating rates and the amount of noise in the data.

VI.   Conclusion

An aeroheating database has been developed for the aerobraking phase of the Mars Reconnaissance Orbiter's mission. Effects of varying density and spacecraft orientation were included in the database. Several parameters were examined in the process of quantifying the uncertainties relating to the aeroheating database. These parameters included the effects of chemical reactions, surface grid refinement, and spacecraft surface temperature. It was

determined that the aeroheating database uncertainty was ±7.9 and ±9.4% with and without the addition of the accommodation coefficient uncertainty. A total of 81 simulations were performed (both DSMC and free molecular) to define the spacecraft aeroheating environment.

The aeroheating database has been compared to heating rates inferred from in-flight data. Several sources of uncertainty have been identified that could have potentially contributed to the discrepancies seen between predicted aeroheating values and those calculated from in-flight temperature sensor data. These uncertainties include values of thermal properties, possible thermal gradients span-wise across the solar panels, radiative input values, the temperature to which the solar panel radiates, and the value of the accommodation coefficient used. The uncertainty for the in-flight data has been estimated to be ±30%. Although there are discrepancies between the aeroheating database and the in-flight values, the overall agreement is favorable. The in-flight peak heating rate was about 15-20% lower than the aeroheating database value. Given the uncertainties associated with the aeroheating database along with the uncertainties associated with the in-flight calculation of the heating rates, this is a reasonable variation between prediction and in-flight values.

References

[1]Wilmoth, R. G., LeBeau, G. J., and Carlson, A. B., "DSMC Grid Methodologies for Computing Low-Density, Hypersonic Flows About Reusable Launch Vehicle," AIAA Paper 96-1812, June 1996.

[2]LeBeau, G. J. and Lumpkin III, F. E., "Application Highlights of the DSMC Analysis Code (DAC) Software for Simulating Rarefied Flows," *Computer Methods in Applied Mechanics and Engineering*, Vol. 191, Issues 6-7, December 7, 2001, pp. 595-609.

[3]Bird, G. A., *Molecular Gas Dynamics and the Direct Simulation of Gas Flows*, Clarendon Press, Oxford, 1994.

[4]Borgnakke, C. and Larsen, P. S., "Statistical Collision Model for Monte Carlo Simulation of Polyatomic Gas Mixture," *Journal of Computational Physics*, Vol. 18, pp. 405-420, 1975.

[5]Moss, J. N., Blanchard, R. C., Wilmoth, R. G. and Braun, R. D., "Mars Pathfinder Rarefied Aerodynamics: Computation and Measurements," *Journal of Spacecraft and Rockets*, Vol. 36, No. 3, May-June 1999, pp. 399-404.

[6]Hollis, B. R., "User's Manual for the One-Dimensional Hypersonic Experimental Aero-Thermodynamic (1DHEAT) Data Reduction Code," NASA CR-4691, August 1995.

[7]Moe, K. and Moe, M. M., "Gas-Surface Interactions and Satellite Drag Coefficients," *Planetary and Space Science*, Vol. 53, 2005, pp. 793-801.